Ray-Tracing-Based 6G Air-to-Indoor Path Loss Modeling in Urban Environments

Yongwan Kim, *Member, IEEE*, and Jungsuek Oh, *Senior Member, IEEE*

***Abstract*—Air-to-indoor (A2I) communication via autonomous aerial vehicles (AAVs) can enhance 6G connectivity. However, most existing studies consider only line-of-sight (LOS) AAV-building links at sub-6 GHz, leaving non-line-of-sight (NLOS) cases and the upper mid-band largely unexplored. In practice, LOS is often infeasible due to flight regulations and, even when available, provides poor lower-floor coverage because of strong elevation-angle dependence. This letter proposes LOS and NLOS A2I path-loss models for the upper mid-band, derived from ray-tracing (RT) simulations that jointly capture outdoor propagation, wall penetration, and indoor loss. Results show that NLOS links, aided by multipath, are less sensitive to elevation and provide more uniform floor coverage, sometimes outperforming high-elevation LOS links, underscoring the need to explicitly incorporate AAV-building NLOS conditions into A2I system design.**

***Index Terms*—Electromagnetic propagation, path loss models, radio propagation, ray-tracing, autonomous aerial vehicle (AAV).**

I. Introduction

CHANNEL modeling above 6 GHz is becoming critical for 6G. In particular, the FR3 upper-mid band (7 GHz to 24 GHz), often termed the "golden band," is a key 6G candidate [1]. Offering wider bandwidth than sub-6 GHz and better coverage than millimeter-wave (mmWave), FR3 provides a favorable tradeoff for next-generation networks [2].

Although FR3 offers wider coverage than mmWave, it still has more limited coverage than sub-6 GHz. To mitigate this, autonomous aerial vehicles (AAVs) can act as aerial base stations (BSs), long-range relays, or mobile data-collecting users [3].

In 5G networks, about 90% of user time and 70% of traffic occur indoors [3]. During emergencies (e.g., earthquakes), wired infrastructure and terrestrial BSs may fail while many users remain trapped in buildings. In such situations, reliable air-to-indoor (A2I) links are crucial, underscoring the need for an accurate A2I channel—especially path loss (PL)—model.

Several studies have investigated A2I PL [4], [5], [6], [7], [8], [9], [10], [11], [12], [13], [14], but mostly at sub-6 GHz and assuming only line-of-sight (LOS) links between the AAV and building, neglecting non-line-of-sight (NLOS) cases. In such LOS-oriented settings, PL strongly depends on elevation angle, often yielding weak signals for lower floors [4]. By contrast, when the AAV is placed in a more distant NLOS position, the lower elevation and additional multipath components can enhance low-floor coverage and yield a more uniform signal distribution across stories. Moreover, maintaining LOS may be impractical due to regulatory constraints (e.g., no-fly zones, altitude limits) or emergency conditions involving fire, heat, and smoke. These factors highlight the importance of NLOS-based AAV communication strategies.

Received 23 December 2025; accepted 19 January 2026. Date of publication 22 January 2026; date of current version 9 April 2026. This work was supported by the Institute of Information & Communications Technology Planning & Evaluation (IITP) grant funded by the South Korea government (MIST) under Grant 2019-0-00098, Advanced and Integrated Software Development for Electromagnetic Analysis. *(Corresponding author: Jungsuek Oh.)*

The authors are with the Institute of New Media and Communications (INMC) and the Department of Electrical and Computer Engineering, Seoul National University, Seoul 08826, South Korea (e-mail: yongwankim@snu.ac.kr; jungsuek@snu.ac.kr).

Digital Object Identifier 10.1109/LAWP.2026.3656909

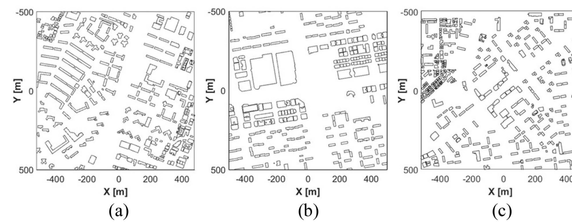

Fig. 1. Selected urban regions in South Korea: (a) Gangnam and (b) Bucheon for PL modeling, and (c) Goyang for model validation.

One way to characterize A2I channels is to measure impulse responses at multiple receiver (Rx) locations, but such site-specific field campaigns are labor-intensive and time-consuming, making large-scale data collection difficult [15].

In contrast, ray-tracing (RT) simulations are widely used to model indoor and outdoor channels, greatly reducing the need for extensive field measurements [15]. In this letter, we propose an upper-mid-band A2I PL model for AAV–building LOS/NLOS conditions, developed using the heterogeneous-computing-based, anxel-beam-shrinkage-method-accelerated image-theory (HAIT) RT [16], [17].

II. Validation of HAIT RT

In this letter, we used a semi-deterministic RT method built on our HAIT framework [16], [17], modeling indoor loss with the 3GPP model instead of HAIT's full 3-D indoor RT. The HAIT engine has been validated against various commercial RT tools and measurement-based studies [16], [17], [18], [19], and finds all physically valid rays, yielding >70% more rays than shooting-and-bouncing-rays (SBR) RT and up to 6051× speedup over existing image-theory (IT)-based RT solvers.

The simulations were performed in three urban areas in South Korea extracted from OpenStreetMap—Gangnam, Bucheon, and Goyang [Fig. 1(a)–(c)]—with building heights of 10 m to 120 m. Gangnam and Bucheon were used to develop the PL models, and Goyang was used for validation.

Prior to detailed A2I PL modeling, HAIT RT was validated by comparing outdoor simulations in Gangnam and Bucheon with the standard 3GPP/ITU-R urban microcell (UMi) PL models in

TABLE I
SIMULATION CONFIGURATIONS FOR OUTDOOR SCENARIOS

Frequency [GHz]	Max. Bouncing #	Tx/RX antenna
6, 12, 18, 24	1, 2, 3, 4, 5, 6 (R: 1-6, D: 1)	Isotropic antenna (vertical polarization)
Number of Tx	Number of Rx	Tx location [m]
1	6,561 per region	(0, 0, 10)
Rx location [m]		
Uniformly distributed on area (x: -400~400 / y: -400~400 / z: 1.5)		

TABLE II
MEAN ERROR OF RT SIMULATION RELATIVE TO 3GPP/ITU-R MODELS

ME [dB]	Max. Bounce #					
	1	2	3	4	5	6
LOS (6 GHz)	2.83	2.86	2.89	2.89	2.89	2.89
NLOS (6 GHz)	-11.7	-4.93	-1.61	0.16	1.07	1.59
LOS (12 GHz)	2.57	2.69	2.71	2.72	2.72	2.72
NLOS (12 GHz)	-13.7	-6.64	-2.89	-0.71	0.53	1.07
LOS (18 GHz)	2.63	2.85	2.91	2.91	2.91	2.90
NLOS (18 GHz)	-15.1	-7.38	-3.61	-1.34	-0.21	0.48
LOS (24 GHz)	2.64	2.86	2.88	2.87	2.87	2.88
NLOS (24 GHz)	-15.9	-8.16	-4.12	-1.76	-0.51	0.09

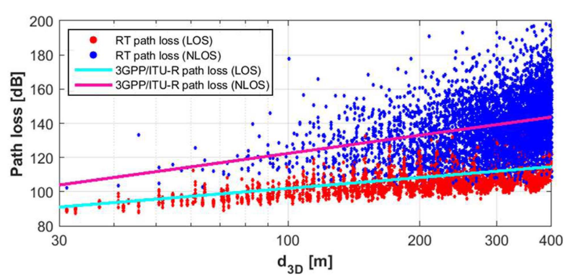

Fig. 2. Comparison of RT PLs and 3GPP/ITU-R models at 24 GHz.

the FR3 band [20], [21], using the RT parameters in Table I. Reflection orders up to six (R = 1–6) and a single diffraction order (D = 1) were considered. HAIT RT uses geometrical optics (GO) [22], [23], [24], [25] and the uniform geometrical theory of diffraction (UTD) [26], [27] for reflection and diffraction, while diffuse scattering is neglected in this work. This is supported by prior work showing that reflection and diffraction alone can reproduce PL without modeling diffuse scattering even at 28 GHz [28], and its impact is expected to be smaller over 6–24 GHz. Buildings and the ground were modeled as concrete and asphalt concrete with dielectric constants of $\varepsilon_r = 5.24$ and 4.83 and conductivities of $\sigma = 0.188$, 0.323, 0.443, and 0.555 S/m (concrete) and $\sigma = 0.132$, 0.348, 0.612, and 0.915 S/m (asphalt concrete) at 6, 12, 18, and 24 GHz, respectively [29].

Table II summarizes the mean errors (MEs) between the 3GPP/ITU-R models and the simulated PL. The ME is defined as $\mathrm{ME} = \sum_{i=1}^{N}(\mathrm{PL}_{\mathrm{model}} - \mathrm{PL}_{\mathrm{RT}})/N$ where N is the number of samples and $\mathrm{PL}_{\mathrm{model}}$ and $\mathrm{PL}_{\mathrm{RT}}$ are the PL values from the 3GPP/ITU-R models and RT, respectively. The MEs converge at five bounces, differing by less than 0.7 dB from six bounces and remaining below 3 dB. Fig. 2 shows LOS and NLOS PL at 24 GHz with six bounces, indicating good agreement with the 3GPP/ITU-R models. The root-mean-square errors (RMSEs) of the 5-bounce RT results relative to the 3GPP/ITU-R models are 6 dB for LOS and 14.9 dB for NLOS, where $\mathrm{RMSE} = \sqrt{\sum_{i=1}^{N}(\mathrm{PL}_{\mathrm{model}} - \mathrm{PL}_{\mathrm{RT}})^2/N}$. These results justify the use of HAIT RT in this study.

Despite MEs below 3 dB relative to the conventional outdoor PL model, we further refined the 3GPP/ITU-R NLOS PL model

TABLE III
SIMULATION CONFIGURATIONS FOR A2I SCENARIOS

Frequency [GHz]	Max. Bouncing #	Tx location [m]
6, 12, 18, 24	5 (R: 5, D: 1)	x: 0, y: 0, z: 30, 55, 80
Rx location [m]		
Uniformly distributed on area (x: -400~400 / y: -400~400 / z: 10, 33.3, 56.6, and 80)		
Number of Rx	Tx/RX antenna	
161,604 per region	Isotropic antenna (vertical polarization)	

by refitting its coefficients using a least-squares method against the RT simulations as follows:

$$\mathrm{PL}'_{\mathrm{UMi-NLOS}} = 11.6 + 38.3\log_{10}(d_{3\mathrm{D}}) + 23.9\log_{10}(f) - 0.3\,(h_{\mathrm{RX}} - 1.5) + X_{\mathrm{SF}}\,(0, \sigma_{\mathrm{UMi-NLOS}})\ [\mathrm{dB}]. \quad (1)$$

Here, $d_{3\mathrm{D}}$ is the Tx–Rx distance, f the frequency in GHz, h_{RX} the Rx height, and X_{SF} a zero-mean Gaussian variable with standard deviation $\sigma_{\mathrm{UMi-NLOS}} = 14.7$. This optimized UMi-NLOS PL model serves as a reference for interpreting the proposed A2I model in Section III.

For reference, we also evaluated an air-to-ground (A2G) configuration in the same UMi environments with the parameters in Table I, except for $h_{\mathrm{TX}} = 80$ m and $h_{\mathrm{RX}} = 10$ m, and compared the results with the 3GPP A2G PL model [30]. Although the A2G models in [30] are defined for LTE bands, the 5-bounce RT simulations yield MEs below 3 dB for both LOS and NLOS, indicating good frequency scalability; the ME differences between 5 and 6 bounces are within 0.23 dB, and the RMSEs are 3.05 dB (LOS) and 12.9 dB (NLOS).

III. A2I PL MODELING AND VALIDATION

A. A2I PL Modeling

Conventional outdoor-to-indoor (O2I) PL models are usually written as the sum of outdoor PL ($\mathrm{PL}_{\mathrm{out}}$), external wall penetration loss ($\mathrm{PL}_{\mathrm{wall,ext}}$), and indoor propagation loss ($\mathrm{PL}_{\mathrm{in}}$) [5], [20], [21]

$$\mathrm{PL} = \mathrm{PL}_{\mathrm{out}} + \mathrm{PL}_{\mathrm{wall,ext}} + \mathrm{PL}_{\mathrm{in}}\ [\mathrm{dB}]. \quad (2)$$

Each component is obtained from separate models. Directly extending this framework to A2I entails several challenges:

1) Lack of Suitable NLOS Outdoor Models: Existing outdoor NLOS models lack the Tx/Rx height range required for A2I; for example, the A2G models in [31] assume ground-level users only and thus cannot capture indoor coverage on upper floors [11].

2) Elevation and Multipath Dependence Under LOS: Even with clear LOS for the AAV-building link, using free-space loss as the $\mathrm{PL}_{\mathrm{out}}$, as in [5], [6], [7], [10], [11], [12], [13], and [14], can be inaccurate. A2I propagation is highly elevation-angle dependent [4], and in practice, multipath from surrounding buildings can sometimes dominate the received power over the steep LOS path, which suffers large floor-penetration loss.

3) Wave Direction Mismatch: Conventional $\mathrm{PL}_{\mathrm{out}}$ models include all rays, even those propagating away from the building. Simply adding $\mathrm{PL}_{\mathrm{out}}$to $\mathrm{PL}_{\mathrm{wall,ext}} + \mathrm{PL}_{\mathrm{in}}$therefore double-counts rays that never enter the building, leading to a physically inconsistent O2I PL.

To address these limitations, we ran integrated A2I simulations with HAIT RT that jointly account for outdoor propagation, wall penetration, and indoor loss in the Gangnam and Bucheon areas of Fig. 1, using the parameters in Table III.

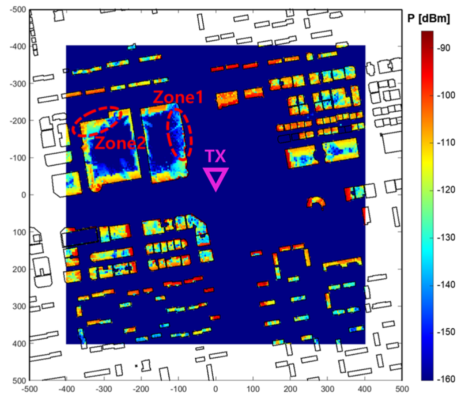

Fig. 3. Simulated received power in Bucheon for $h_{RX} = 10$ m, $h_{TX} = 80$ m, $f = 24$ GHz, low-loss penetration model, and 1 W transmit power.

External wall penetration was modeled using the low-/high-loss model in [20] plus incident-angle dependent loss in [32]

$$\mathrm{L_{Low}} = 5 - 10\log_{10}\left(0.3 \cdot 10^{-\frac{2+0.2f}{10}} + 0.7 \cdot 10^{-\frac{5+4f}{10}}\right) \text{ [dB]} \quad (3)$$

$$\mathrm{L_{High}} = 5 - 10\log_{10}\left(0.7 \cdot 10^{-\frac{25.4+0.11f}{10}} + 0.3 \cdot 10^{-\frac{5+4f}{10}}\right) \text{ [dB]} \quad (4)$$

$$\mathrm{L}_e(\theta) = 0.212\,|\theta| \quad (5)$$

where θ is incident angle in degrees. Since $\mathrm{L_{Low}}$ and $\mathrm{L_{High}}$ denote angle-averaged penetration loss, we set them to the loss at 45° incidence. Accordingly, the penetration loss models used in RT are as follows:

$$\mathrm{L_{Low,RT}} = \mathrm{L_{Low}} - \mathrm{L}_e(45^\circ) + \mathrm{L}_e(\theta) \text{ [dB]} \quad (6)$$

$$\mathrm{L_{High,RT}} = \mathrm{L_{High}} - \mathrm{L}_e(45^\circ) + \mathrm{L}_e(\theta) \text{ [dB]}. \quad (7)$$

Indoor propagation loss was set to 0.5 dB/m and internal wall penetration was neglected, following [20], [21], [33], yielding mean PL errors below 6 dB with respect to the measurements in [33]. Floor penetration was also considered: according to [34], upper-mid-band penetration losses are about 52, 62, and 67 dB for 1–3 floors, far exceeding indoor attenuation without floor penetration (0.5 dB/m). Floor-penetrating rays were therefore treated as negligible by setting floor penetration loss to infinity. Because the actual floor spacing is unknown, a uniform spacing of 3 m was assumed and rays exceeding this vertical distance were terminated. All other parameters followed the outdoor scenario in Section II.

Fig. 3 shows the received-power distribution in Bucheon at $z = 10$ m and 24 GHz with $h_{TX} = 80$ m, using $\mathrm{L_{Low,RT}}$ and 1 W transmit power. As expected, some NLOS regions exhibit stronger received power than nearby LOS areas. For example, Zone 2 (NLOS) yields higher power than Zone 1 (LOS) despite being farther from the Tx: in Zone 1, the direct path suffers severe loss due to a large incident angle and multiple floor penetrations, and the lack of nearby buildings limits multipath, whereas Zone 2 benefits from rich reflections from surrounding buildings with low incident and elevation angles, which strengthen the signal. These results indicate that AAV-building NLOS configurations can be advantageous for A2I links, especially under flight-zone or altitude constraints.

The proposed A2I PL model extends the alpha–beta–gamma model [20], [21] by adding elevation-angle- and indoor-distance–dependent terms. Its coefficients are obtained via ordinary least squares [35] from RT results for buildings within 400 m (horizontal length) from the Tx. The resulting model, incorporating the low-loss term $\mathrm{L_{Low,RT}}$, is given by:

$$\mathrm{PL}^{\mathrm{Low}}_{\mathrm{building,\ LOS}} = 43.4 + 17.0\log_{10}(d_{\mathrm{TR}}) + 27.1\log_{10}(f) + 39.8\,|\theta_{\mathrm{elev}}| + 0.4 d_{\mathrm{2D,in}} + X_{\mathrm{SF}}(0, \sigma_{\mathrm{building,LOS}}) \text{ [dB]}. \quad (8)$$

$$\mathrm{PL}^{\mathrm{Low}}_{\mathrm{building,\ NLOS}} = 11.5 + 39.9\log_{10}(d_{\mathrm{TR}}) + 30\log_{10}(f) + 4.2\,|\theta_{\mathrm{elev}}| + 0.9 d_{\mathrm{wall,ext,2D}} + X_{\mathrm{SF}}(0, \sigma_{\mathrm{building,NLOS}}) \text{ [dB]}. \quad (9)$$

Here, $\mathrm{PL}^{\mathrm{Low}}_{\mathrm{building,\ LOS}}$ denotes the PL when the Tx–Rx path crosses only one external wall, whereas $\mathrm{PL}^{\mathrm{Low}}_{\mathrm{building,NLOS}}$ applies otherwise. d_{TR} is the 3D Tx–Rx distance, $d_{\mathrm{2D,in}}$ the indoor horizontal propagation length along the Tx–Rx path, and $d_{\mathrm{wall,ext,2D}}$ the shortest horizontal distance from the Rx to the nearest external wall. The indoor-distance metric differs between LOS and NLOS because LOS links are dominated by a single direct path, whereas NLOS links are governed by multipath components arriving from various directions. θ_{elev} is the Tx–Rx elevation angle in radians.

The constant and frequency-dependent coefficients of $\mathrm{PL}^{\mathrm{Low}}_{\mathrm{building,\ LOS}}$ (43.4 and 27.1) exceed those of the free-space PL (FSPL), which is defined as [14]

$$\mathrm{FSPL} = 32.44 + 20\log_{10}(d_{\mathrm{3D}}) + 20\log_{10}(f) \text{ [dB]}. \quad (10)$$

This is because $\mathrm{PL}^{\mathrm{Low}}_{\mathrm{building,\ LOS}}$ inherently includes both $\mathrm{PL_{wall,ext}}$ and its frequency dependence. The coefficient associated with outdoor PL exponent (17.0) is slightly smaller than that of FSPL, since d_{TR} spans both outdoor and indoor segments, whereas d_{3D} represents only the outdoor path. As expected, $\mathrm{PL}^{\mathrm{Low}}_{\mathrm{building,\ LOS}}$ shows strong elevation dependence (39.8), yielding nearly 56 dB of additional loss at 80°, and the horizontal indoor-loss coefficient of 0.4 is close to the indoor attenuation used in the RT simulations, which is reasonable because elevation effects are captured by a separate term.

For $\mathrm{PL}^{\mathrm{Low}}_{\mathrm{building,NLOS}}$, the constant and distance coefficients (11.5 and 39.9) are close to those of the UMi ground-BS model in (1) (11.6 and 38.3). This results from offsetting effects: although the AAV–building link experiences less outdoor blockage (lower PL) than a ground-BS scenario due to the higher h_{TX}, the outdoor-loss term of the proposed A2I model is dominated by indoor Rxs in buildings along narrow, building-dense streets with severe blockage and high outdoor loss, where most indoor Rxs are located, whereas conventional ground-BS models are dominated by Rxs along wide streets with lower PL [36]. The frequency-dependent term (30) exceeds that of $\mathrm{PL}^{\mathrm{Low}}_{\mathrm{building,LOS}}$ (27.1), reflecting stronger frequency dependence of reflection and diffraction in multipath propagation. Its elevation coefficient (4.2) is much smaller than that of $\mathrm{PL}^{\mathrm{Low}}_{\mathrm{building,LOS}}$ (39.8), since dominant multipath components generally arrive with smaller elevation angles than the direct AAV–Rx path. Finally, the perpendicular horizontal indoor-loss coefficient (0.9) is larger than the 0.5 dB/m indoor attenuation used in the RT setup, which can be attributed to oblique incidence effects.

The shadowing factors $\sigma_{\mathrm{building,LOS}}$ and $\sigma_{\mathrm{building,NLOS}}$ are 14.5 dB and 14.0 dB, respectively. The larger LOS shadowing factor relative to the standard UMi ground-BS case arises because, inside LOS buildings, some regions cannot be reached by the direct Tx ray due to floor penetration loss, so their PL is

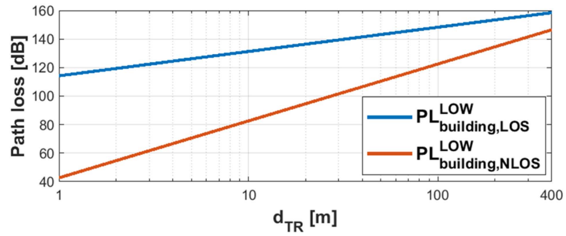

Fig. 4. LOS and NLOS building path loss at 6 GHz (with $d_{2D,in} = d_{wall,ext,2D} =$ 3m and $\theta_{elev} = 1.22$, i.e., 70°).

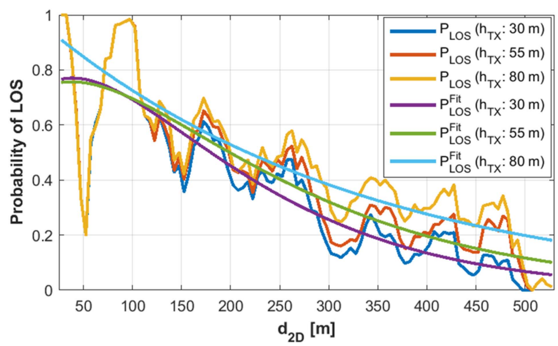

Fig. 5. Simulated and fitted LOS probabilities in Gangnam and Bucheon.

dominated by multipath. As a result, LOS buildings contain a mixture of direct-ray-dominant and multipath-dominant areas, which increases the overall shadowing variance.

$PL^{Low}_{building,\ LOS/NLOS}$ are defined under the low-loss condition. In the high-loss case, the only change is the average external wall penetration loss (L_{Low} versus L_{High}). Since $L_{High} - L_{Low}$ varies by less than 1.3 dB over 6 GHz to 24 GHz, the high-loss models are obtained by simply adding median value of $L_{High} - L_{Low}$ over the band (18.2 dB) to $PL^{Low}_{building,LOS/NLOS}$, i.e.,

$$PL^{High}_{building,\ LOS} = 61.6 + 17.0\log_{10}(d_{TR}) + 27.1\log_{10}(f) + 39.8\,|\theta_{elev}| + 0.4d_{2D,in} + X_{SF}(0, \sigma_{building,LOS})\ \text{[dB]} \quad (11)$$

$$PL^{High}_{building,\ NLOS} = 29.7 + 39.9\log_{10}(d_{TR}) + 30\log_{10}(f) + 4.2\,|\theta_{elev}| + 0.9d_{wall,ext,2D} + X_{SF}(0, \sigma_{building,NLOS})\ \text{[dB]}. \quad (12)$$

Fig. 4 shows the $PL^{Low}_{building,LOS/NLOS}$ at 6 GHz with $d_{2D,in} = d_{wall,ext,2D} = 3\,\text{m}$ and a large elevation angle $\theta_{elev} = 1.22$ rad (70°). As expected, $PL^{Low}_{building,LOS}$ exceeds $PL^{Low}_{building,NLOS}$, highlighting the benefit of NLOS-based A2I communication.

We analyzed the LOS probability in the Gangnam and Bucheon. A link is classified as LOS if the Tx–Rx direct path penetrates only one external wall, and as NLOS otherwise. As shown in Fig. 5, we obtained the LOS probability as a function of h_{TX} and horizontal distance d_{2D} from the Tx, and fitted it with exponential models following [28] for each h_{TX}:

$$P^{Fit}_{LOS}\big|_{30m} = -30.18791e^{-0.00893d_{2D}} + 30.90250e^{-0.00862d_{2D}} \quad (13)$$

$$P^{Fit}_{LOS}\big|_{55m} = -1.25075e^{-0.01056d_{2D}} + 1.96813e^{-0.00554d_{2D}} \quad (14)$$

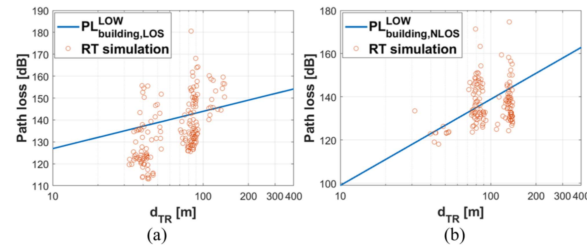

Fig. 6. Comparison between the proposed A2I PL models and RT-simulated PL in Goyang at 24 GHz: (a) LOS links and (b) NLOS links.

$$P^{Fit}_{LOS}\big|_{80m} = -7.45471e^{-0.00399d_{2D}} + 8.44401e^{-0.00388d_{2D}}. \quad (15)$$

The coefficients were derived using MATLAB's nonlinear least-squares solver *lsqcurvefit*, and the RMSEs between the fitted and simulated probabilities are 0.12, 0.13, and 0.13 for $h_{TX} = 30, 55, 80$ m, respectively.

B. Model Validation

With the parameters in Table I, RT simulations in Goyang [Fig. 1(c)] yield MEs $\leq$ 3.5 dB and LOS/NLOS RMSEs of 6.2/14.4 dB relative to the UMi ground-BS 3GPP/ITU-R PL models [20], [21] (5 bounces), confirming Goyang as a typical UMi environment comparable to Gangnam and Bucheon.

Next, we performed A2I simulations in Goyang using the same parameters as in Table III with $L_{Low,RT}$ and compared the simulated PL with the $PL^{Low}_{building,\ LOS/NLOS}$. The MEs were 3.45 dB (LOS) and 2.72 dB (NLOS), and the RMSEs were 10.2 dB and 12.9 dB, respectively, indicating satisfactory validation. The ME close to 3 dB likely reflects differences in building-height distributions between Gangnam/Bucheon and Goyang. Fig. 6 compares the simulated PL for Goyang with $PL^{Low}_{building,LOS}$ and $PL^{Low}_{building,NLOS}$: Fig. 6(a) shows $PL^{Low}_{building,LOS}$ for $\theta_{elev} = 35°$, 24 GHz, and $d_{2D,in} =$ 12 m, together with LOS RT samples for $\theta_{elev} = 30°$–40°, 24 GHz, and $d_{2D,in} =$ 5–19 m; Fig. 6(b) shows $PL^{Low}_{building,NLOS}$ for $\theta_{elev} = 35°$, 24 GHz, and $d_{wall,ext,2D} =$ 4 m, together with NLOS RT samples for $\theta_{elev} = 30°$–40°, 24 GHz, and $d_{wall,ext,2D} =$ 0–8 m.

IV. Conclusion

This letter presents LOS and NLOS A2I PL models for the FR3 band, derived from HAIT RT simulations. Unlike conventional O2I formulations, the model jointly accounts for outdoor propagation, wall penetration, and indoor loss to overcome limitations of existing approaches. The model's coefficients are further optimized via ordinary least squares using large-scale simulations in two urban environments.

The results show that the model captures key differences between LOS and NLOS cases: LOS links are strongly elevation-dependent, whereas NLOS links benefit from multipath and can even provide better coverage on lower floors than LOS links. These findings indicate that AAV-building NLOS links are a viable strategy under realistic flight or emergency constraints and should be considered in A2I system design.

REFERENCES

[1] S. Kang et al., “Cellular wireless networks in the upper mid-band,” *IEEE Open J. Commun. Soc.*, vol. 5, pp. 2058–2075, 2024.

[2] D. Shakya et al., “Comprehensive FR1(C) and FR3 lower and upper mid-band propagation and material penetration loss measurements and channel models in indoor environment for 5G and 6G,” *IEEE Open J. Commun. Soc.*, vol. 5, pp. 5192–5218, 2024.

[3] J. Cui, B. Hu, and S. Chen, “Resource allocation and location decision of a UAV-relay for reliable emergency indoor communication,” *Comput. Commun.*, vol. 159, pp. 15–25, 2020.

[4] L. Norberti, R. Nebuloni, and M. Magarini, “Characterization of the indoor-to-outdoor wireless channel in air-to-ground communication systems,” in *Proc. 16th Int. Conf. Wireless Mobile Comput., Netw. Commun.*, Thessaloniki, Greece, 2020, pp. 1–6.

[5] K. Saito, Q. Fan, N. Keerativoranan, and J.-I. Takada, “Vertical and horizontal building entry loss measurement in 4.9 GHz band by unmanned aerial vehicle,” *IEEE Wireless Commun. Lett.*, vol. 8, no. 2, pp. 444–447, Apr. 2019.

[6] A. H. Sawalmeh, N. S. Othman, H. Shakhatreh, and A. Khreishah, “Wireless coverage for mobile users in dynamic environments using UAV,” *IEEE Access*, vol. 7, pp. 126376–126390, 2019.

[7] T.-Y. Kim, Y. Ahn, J. Lee, and J.-H. Kim, “Joint movement and user association of UAV-BS for indoor user service: A multi-agent deep reinforcement learning approach,” in *Proc. IEEE 22nd Consum. Commun. Netw. Conf.*, Las Vegas, NV, USA, 2025, pp. 1–4.

[8] K. Saito, Q. Fan, N. Keerativoranan, and J.-I. Takada, “Site-specific propagation loss prediction in 4.9 GHz band outdoor-to-indoor scenario,” *Electronics*, vol. 8, no. 12, 2019, Art. no. 1398.

[9] J. Kang, K. Kim, H. Lee, and J.-H. Kim, “Lyapunov optimization-based online positioning in UAV-assisted emergency communications,” *IEEE Access*, vol. 11, pp. 60835–60843, 2023.

[10] J. Cui, H. Shakhatreh, B. Hu, S. Chen, and C. Wang, “Power-efficient deployment of a UAV for emergency indoor wireless coverage,” *IEEE Access*, vol. 6, pp. 73200–73209, 2018.

[11] H. Shakhatreh, A. Khreishah, and I. Khalil, “Indoor mobile coverage problem using UAVs,” *IEEE Syst. J.*, vol. 12, no. 4, pp. 3837–3848, Dec. 2018.

[12] J. Kang, H. Kashihara, J. T. S. Sumantyo, and J.-H. Kim, “Performance analysis of Uplink NOMA based full-duplex UAV for indoor disaster environment,” in *Proc. Int. Conf. Inf. Commun. Technol. Convergence*, Jeju Island, Korea, Republic of, 2021, pp. 245–247.

[13] H. Shakhatreh, A. Khreishah, and B. Ji, “Providing wireless coverage to high-rise buildings using UAVs,” in *Proc. IEEE Int. Conf. Commun.*, Paris, France, 2017, pp. 1–6.

[14] C. Ge, D. Zhai, R. Zhang, and J. Jiang, “Statistical characteristics of excess loss for UAV-to-indoor propagation channel,” in *Proc. IEEE Globecom Workshops*, Kuala Lumpur, Malaysia, 2023, pp. 1481–1486.

[15] J.-H. Lee, J.-S. Choi, J.-Y. Lee, and S.-C. Kim, “28 GHz millimeter-wave channel models in urban microcell environment using three-dimensional ray tracing,” *IEEE Antennas Wireless Propag. Lett.*, vol. 17, no. 3, pp. 426–429, Mar. 2018.

[16] Y. Kim, H. Yang, H. Kim, J. Jo, and J. Oh, “Anxel beam shrinkage method and heterogeneous computing-accelerated full-image theory method ray tracing enabling massive outdoor propagation modeling,” *IEEE Trans. Antennas Propag.*, vol. 72, no. 7, pp. 5935–5949, Jul. 2024.

[17] Y. Kim, H. Kim, J. Lee, H. Cho, and J. Oh, “Transmission-integrated HAIT ray tracing for massive O2I propagation modeling with MTN preprocessing and Anxel beam transformation,” *IEEE Trans. Antennas Propag.*, vol. 73, no. 11, pp. 9255–9270, Nov. 2025.

[18] H. Yang et al., “Beyond limitations of 5G with RIS: Field trial in a commercial network, recent advances, and future directions,” *IEEE Commun. Mag.*, vol. 62, no. 10, pp. 132–138, Oct. 2024.

[19] H. Yang et al., “6G channel measurement in urban, dense urban scenario and massive ray-tracing-based coverage analysis at 7.5 GHz,” in *Proc. IEEE Int. Conf. Commun.*, Montreal, QC, Canada, 2025, pp. 3309–3314.

[20] 3GPP TR 38.901 v19.1.0, Study on channel model for frequencies from 0.5 to 100 GHz, Sep. 2025.

[21] ITU, Guideline for evaluation of radio interface technologies for IMT-2020, Rep. ITU-R M.2412-0, Oct. 2017.

[22] C. A. Balanis, *Advanced Engineering Electromagnetics*. New York, NY, USA: Wiley, 1989.

[23] R. Brem and T. F. Eibert, “A shooting and bouncing ray (SBR) modeling framework involving dielectrics and perfect conductors,” *IEEE Trans. Antennas Propag.*, vol. 63, no. 8, pp. 3599–3609, Aug. 2015.

[24] J. E. Roy, “New results for the effective propagation constants of nonuniform plane waves at the planar interface of two lossy media,” *IEEE Trans. Antennas Propag.*, vol. 51, no. 6, pp. 1206–1215, Jun. 2003.

[25] Y. Kim, H. Yang, and J. Oh, “Critical angle formulation of nonuniform plane waves for determining correct refraction angles at planar interface,” *IEEE Trans. Antennas Propag.*, vol. 71, no. 3, pp. 2861–2866, Mar. 2023.

[26] R. G. Kouyoumjian and P. H. Pathak, “A uniform geometrical theory of diffraction for an edge in a perfectly conducting surface,” *Proc. IEEE*, vol. 62, no. 11, pp. 1448–1461, Nov. 1974.

[27] P. Bernardi, R. Cicchetti, and O. Testa, “A three-dimensional UTD heuristic diffraction coefficient for complex penetrable wedges,” *IEEE Trans. Antennas Propag.*, vol. 50, no. 2, pp. 217–224, Feb. 2002.

[28] J.-H. Lee, J.-S. Choi, and S.-C. Kim, “Cell coverage analysis of 28 GHz millimeter wave in urban microcell environment using 3-D ray tracing,” *IEEE Trans. Antennas Propag.*, vol. 66, no. 3, pp. 1479–1487, Mar. 2018.

[29] International Telecommunications Union Radiocommunication Sector. Effects of building materials and structures on radio-wave propagation in the range of 1 MHz to 450 GHz. Recommendation P.2040-4. ITU-R, approved Sep. 23, 2025.

[30] 3GPP TR 36.777 v15.0.0, Study on enhanced LTE support for aerial vehicles, Dec. 2017.

[31] A. Al-Hourani, S. Kandeepan, and A. Jamalipour, “Modeling air-to-ground path loss for low altitude platforms in urban environments,” in *Proc. IEEE Glob. Commun. Conf.*, Austin, TX, USA, 2014, pp. 2898–2904.

[32] ITU, Prediction of building entry loss, Recommendation ITU-R P.2109-2, Aug. 2023.

[33] P. Koivumäki, A. Karttunen, and K. Haneda, “Ray-optics simulations of outdoor-to-indoor multipath channels at 4 and 14 GHz,” *IEEE Trans. Antennas Propag.*, vol. 71, no. 7, pp. 6046–6059, Jul. 2023.

[34] M. Sasaki et al., “Path loss model to evaluate interference for small cells between different floors,” *Nippon Telegraph Telephone Corp. (NTT) Tech. Rev.*, vol. 15, no. 7, pp. 1–4, Jul. 2017.

[35] S. Weisberg, *Applied Linear Regression*. New York, NY, USA: Wiley, 2013.

[36] N. Moraitis and K. S. Nikita, “Ray-tracing propagation modeling in urban environment at 140 GHz for 6G wireless networks,” *IEEE Access*, vol. 11, pp. 133835–133849, 2023.